J Mol Model (2014) 20:2485
DOI 10.1007/s00894-014-2485-0

ORIGINAL PAPER

Conformation and dynamics of 8-Arg-vasopressin in solution

Elke Haensele · Lee Banting · David C. Whitley · Timothy Clark

Received: 21 August 2014 / Accepted: 6 October 2014 / Published online: 6 November 2014

Abstract Arginine-vasopressin was subjected to a long (11 μs) molecular dynamics simulation in aqueous solution. Analysis of the results by DASH and principal components analyses revealed four main ring conformations that move essentially independently of the faster-moving tail region. Two of these conformations (labeled "saddle") feature well-defined β-turns in the ring and conserved transannular hydrogen bonds, whereas the other two ("open") feature neither. The conformations have been identified and defined and are all of sufficient stability to be considered candidates for biological conformations in their cognate receptors.

Keywords Vasopressin · Molecular dynamics · DASH analysis · Peptides · Principal component analysis

Introduction

8-Arginine-vasopressin [AVP, also known simply as vasopressin (VP), antidiuretic hormone (ADH) or argipressin]—one of the first biologically active peptides to be synthesized by du Vigneaud in 1954 [1]—is a nonapeptide with a six-membered cyclic moiety (Cys^1-Tyr^2-Phe^3-Gln^4-Asn^5-Cys^6) closed by a Cys^1-Cys^6 disulfide bridge, and an α-amidated three-residue tail (Pro^7-Arg^8-Gly^9-NH_2).

AVP is a neurohypophyseal hormone and belongs to the vasopressin family of the evolutionary lineage vasotocin-vasopressin. Vasopressin-like hormones are found in all vertebrates, with AVP being the mammalian form. They all possess a basic amino acid, such as arginine or lysine, in position eight and are all involved in water homeostasis (for reviews see, inter alia [2–4]).

AVP is synthesized in the magnocellular neurons of the posterior pituitary gland [5] complexed with neurophysin (NP), its carrier protein [6]. The function of NP is to target, package and store AVP before release into the bloodstream [3]. The receptors activated by AVP belong to the transmembrane G-protein coupled receptor (GPCR) superfamily [2].

Once secreted into the blood stream, AVP is implicated in myriad physiological functions within the endocrine and neurocrine systems. Examples of its hormone function in addition to water homeostasis [2–4] include regulation of blood pressure [7, 8], antipyretic [9] and analgesic effects [10]. AVP acts as a secretagogue for adrenocorticotropin [3, 11, 12], glucagon and insulin [13]. The peptide is thought to mediate social and sexual behavior, especially aggression, anxiety and pair-bonding [14]. Furthermore, AVP is believed to enhance memory and facilitate learning [3] and to be involved in the pathophysiology of clinical disorders such as autism [15], and may even play a role in circadian rhythm misalignments like jet lag [16].

Lowered AVP release in humans effects an increased blood sodium concentration (hypernatremia), excessive urine production (polyuria) and thirst. This may in turn lead to diabetes insipidus treatable by administration of AVP and AVP analogs [17]. In contrast, heightened AVP release causes hyponatremia, which may result in brain disease and lung cancer [18, 19] and can be treated with AVP-receptor

Electronic supplementary material The online version of this article (doi:10.1007/s00894-014-2485-0) contains supplementary material, which is available to authorized users.

E. Haensele · L. Banting · D. C. Whitley · T. Clark (✉)
Centre for Molecular Design, School of Pharmacy and Biomedical Sciences, University of Portsmouth, Portsmouth PO1 2DT, UK
e-mail: tim.clark@fau.de

T. Clark
Computer-Chemie-Centrum and Interdisciplinary Center for Molecular Materials, Friedrich-Alexander-Universität Erlangen-Nürnberg, Nägelsbachstraße 25, 91052 Erlangen, Germany

antagonists [20]. AVP can be used in emergency medicine as an alternative to epinephrine in the event of cardiac arrest [21].

To date, the only fully resolved crystal structure of AVP is as part of a trypsin complex (PDB ID: 1YF4) [22]. This structure contains a markedly different backbone conformation to those found for the closely related peptide hormones 8-Lys-vasopressin (LVP, PDB ID: 1JK4 [6]) and oxytocin (OT, PDB ID: 1NPO [23]) in their NP-complexes in the solid state.

The conformational characteristics of the peptide structures in the physiologically relevant neurophysin-complexes are a saddle-like ring with β-turns involving residues 3,4/4,5 and a high occurrence of transannular hydrogen bonds, primarily between Tyr^2O and Asn^5NH (cf. Scheme 1b). The tripeptide tail is resolved only in the OT-NP complex (PDB ID: 1NPO) where it is folded and possibly stabilized by a hydrogen bond Cys^6O-Gly^9NH (cf. Scheme 2b).

NMR studies suggest rapid interchange between the β-turn conformations of AVP in solution, although a folded (*saddle*) geometry appears to be maintained [24]. The polarity of the solvent seems only to affect formation of intramolecular hydrogen bonds. In DMSO, a hydrogen bond is indicated between Tyr^2O and Asn^5NH [24] but apparently not in water [25]. Studies in SDS micelles suggest the hydrophilic regions of the ring interact with a membrane, while the hydrophobic tail is exposed to the aqueous phase. Again, in this study the cyclic backbone of the AVP ring attached to the micelles appears similar to the NP-complexed form [26].

These saddle-like conformations with a strongly puckered ring and the β-turns mentioned above have been confirmed computationally as "low-energy conformations" inter alia by Liwo et al. [27] via Monte Carlo and molecular dynamics (MD) simulations.

In contrast, the conformation of AVP within the trypsin complex (PDB ID: 1YF4) is characterized by an unfolded, more planar ring conformation, here designated as "open", with no significant internal hydrogen bonds and an extended tail (cf. Scheme 1a). AVP is an efficient inhibitor of trypsin [22], although this is not known to be a true physiological function of AVP. The *open* conformation adopted in this trypsin complex can nevertheless be regarded as a bioactive conformation. To our knowledge, little attention has been paid to an *open* conformation or its potential role in receptor binding with the vasopressin-receptor V2R [28].

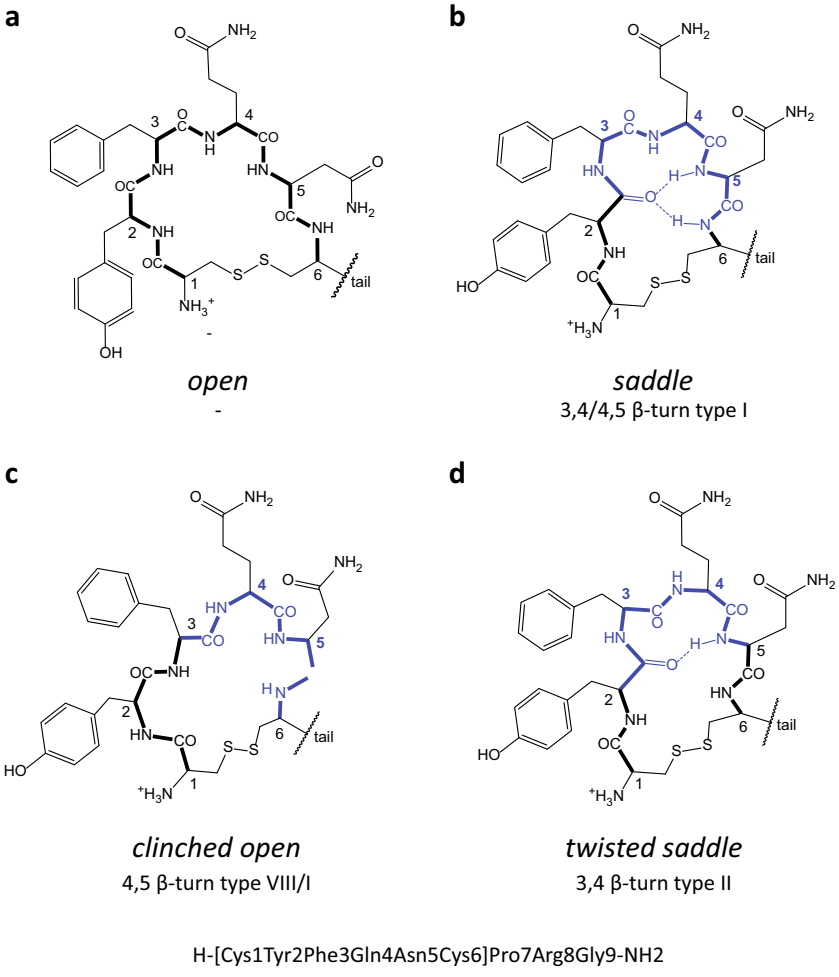

Scheme 1a–d Main conformational types of the cyclic part of 8-Arg-vasopressin (AVP). **a** *Open*: no intramolecular hydrogen bonds and no classical β-turn types. **b** *Saddle*: β-turn type I centered at 3,4/4,5 and stabilized by a transannular hydrogen bond from Tyr^2O to Asn^5NH and Cys^6NH. **c** *Clinched open*: minor propensity for β-turns type VIII or I centered at 4,5. **d** *Twisted saddle*: β-turn type II centered at 3,4 with hydrogen bond Tyr^2O to Asn^5NH

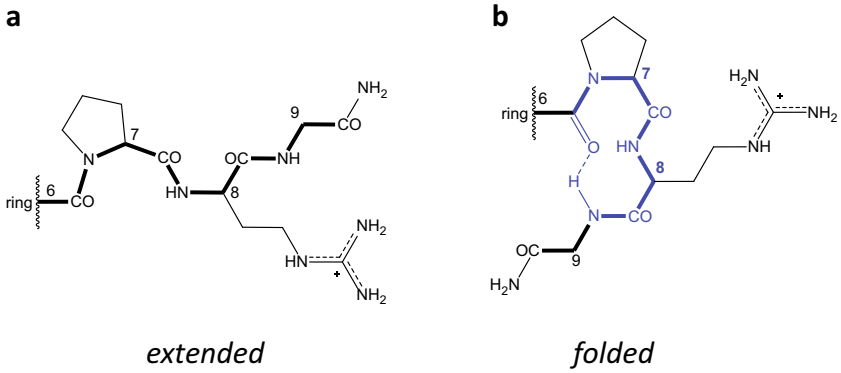

H-[Cys1Tyr2Phe3Gln4Asn5Cys6]Pro7Arg8Gly9-NH2

Scheme 2a,b Main conformational types of the N-terminal tail of AVP. **a** *Extended* tail: no turns, no significantly populated hydrogen bonds. **b** *Folded* tail: β-turn type II centered at residues 7 and 8, hydrogen bond from Cys^6O to Gly^9NH

The V2R agonist-binding-pocket, common to all VP and OT receptor types, is located in a cleft within the transmembrane (TM) domains and AVP has been proposed to be buried almost completely within the receptor channel [28, 29]. The hydrophobic ring-residues (Cys^1-Tyr^2-Phe^3) are predicted to interact with residues of the TM-helices to activate signal transduction, while the tail points outside the TM-core, interacting with an extracellular loop via its hydrophilic residue Arg^8. The interaction between Arg^8 and the extracellular loops is also thought to be key to receptor recognition [2, 30].

Current models for interactions of peptide hormones with their receptors suggest multi-step mechanisms in which the peptide first contacts the cell membrane and then diffuses to the receptor until it finally finds its position to trigger receptor activities [31, 32]. These events are probably accompanied by conformational changes of the ligand and concomitant allosteric effects on the receptors [33]. A flexible ligand exists in solution as an equilibrium involving several conformations of differing bioactivities. A conformation that has not yet been recognized with "slow" experimental techniques, such as NMR, might nevertheless be the important conformation for triggering biological effects such as receptor recognition and activation or inhibition [33–35].

Thus, we have now investigated the conformational dynamics of this peptide in solution in depth with modern computational methods and analysis tools with special regard to the *open* conformation, which is evident in the largely ignored 1YF4 X-ray structure of AVP and is significantly different from the known *saddle* conformation.

MD simulations have proven an accurate tool for describing the atomistic details of the conformational dynamics of biological systems in solution (e.g., [36]). Rapidly developing computational methods, increasing computational performance and improved force fields now make it possible to reveal new structural aspects of systems such as AVP, especially because microsecond simulations are now possible for a peptide of this size.

We now report an unrestrained 11 μs MD simulation of the AVP-1YF4-peptide in explicit water solvent at 300 K using AMBER 10 [37] and a detailed analysis of the resulting conformational space with several analysis tools contained in Ptraj [38] and DASH [39]—a fast conformational analysis tool for MD simulations developed especially for long trajectories for which classical clustering algorithms scale poorly.

Methods

Molecular dynamics simulation

The AMBER10 program suite [37] was used to optimize geometries and for the MD simulations. The X-ray structure of AVP from the trypsin complex (PDB ID: 1YF4) [22] was chosen as the initial conformation. The peptide was placed in a truncated octahedron water box [box size (XYZ) =38.97 $Å^3$] using the TIP4P-Ew water model [40, 41]. Two chloride counterions were added to neutralize the system. The simulation system consisted of a total of 4,792 atoms, including 1,162 four-site water molecules and 142 AVP atoms.

The system was optimized using 500 steps of steepest-descent optimization followed by 8,945 of conjugated-gradient minimization at constant volume.

MD simulations were carried out using the AMBER ff99SB force field [42] under constant temperature (T = 300 K, Berendsen coupling [43] of 1.0 ps to an external heat bath) and constant pressure (p = 1 atm) periodic boundary conditions with a non-bonded cut off of 8 Å. The SHAKE [44] algorithm was employed for hydrogen atoms with a simulation time step of 2 fs. Energies were calculated using the particle mesh Ewald (PME) method [45] and coordinate 'snapshots' were written every picosecond. AVP was simulated in explicit water at 300 K for 11 μs.

DASH analysis

Conformational clustering was performed with DASH, version 2.10 [39]. DASH is a fast conformational analysis tool for MD simulations developed especially for long trajectories for which classical pairwise distance-metric clustering algorithms (Cα) scale poorly. It analyses time-series of torsion angles, e.g., the trajectories of the Φ/Ψ dihedral angles of the protein/peptide backbone during the MD simulation. The result is a time series of DASH states called a DASH state trajectory. A DASH state is simply an ensemble of torsion angles that is representative for a main conformation (equivalent to a conformational cluster). No predetermined number of states is required, in contrast to clustering algorithms that use a similarity matrix, such as those implemented in AMBER tools [38]. A conformation must persist for a minimum number of time steps before it is identified as a DASH state, which gives an accurate representation of significant conformational changes. The DASH software is released under the terms of the GNU general public license and can be downloaded from the University of Portsmouth website [46].

Principal component analysis

The principal component (PC) analysis (PCA) was conducted using the dihedral angles extracted from the simulation (11,000 snapshots) using SAR-caddle [47]. Kaiser's eigenvalue-one test [48] was used to determine the number of significant PCs. Weights are simply the squares of the coefficients of the torsional angles in the relevant PC-eigenvector.

Further details of the calculations and analyses are given in the Supporting Information.

Results and discussion

Ring conformations

Trajectory (transitions)

An 11 μs MD simulation of AVP in solution reveal the high conformational flexibility and fluctuation of this peptide (see Video S1). Figure 1a shows the trajectory of conformational changes of the Cα-backbone atoms 1–9 of AVP as root mean square deviation (RMSD) from the minimized starting conformation (PDB ID: 1YF4). Average RMSD values of distinct time-windows from the trajectory are given in Table 1. Significant RMSD changes indicate significant conformational changes, but despite a high fluctuation, there were few substantial RMSD changes during the 11 μs MD simulation. The most obvious transition was at 1.46 μs. Limiting the RMSD calculation either to the ring (Fig. 1b) or to the tail Cα-atoms (Fig. 1d) shows that the major overall transition of the peptide (Fig. 1a) corresponds to a change of the ring conformation. The radius of gyration of the ring system (Fig. 1c) revealed further distinct transitions between differently folded ring conformations at 5.90, 6.43 and 7.19 μs. The tail, however, fluctuated with a much higher frequency, apparently between two conformational states that are distributed evenly over the simulation. The video clip (Video S1) suggests that these two tail states may be assigned to an extended state (Scheme 2a), in which the tail points away from the ring, and a folded state (Scheme 2b) in which the tail turns towards the lower face of the ring. The high frequency of transitions between the two tail states indicated a high flexibility of the tail, significantly higher than the ring.

DASH state analysis

A DASH analysis of all 16 Φ/Ψ dihedral angles (T16) of the AVP backbone (Cα 2 to 9) during the 11 μs MD simulation results in 35 conformational states. Every DASH state represents, like a cluster, a conformation that is representative for an ensemble of similar backbone conformations. The 35 overall states can be clustered into four groups of states with common structural characteristics for the cyclic part of the peptide (Fig. 2a–d) and a fifth group of states ("variants", Figure S1 and Table S1) that does not match one of the main groups. This fifth group occurs between 5.90 and 6.43 μs. A detailed table of the sequence of DASH states (DASH state trajectory) during the 11 μs simulation is available as Supplementary Material (Table S2).

DASH ring-state analysis

As the RMSD trajectories suggest that the tail movements do not affect the main ring conformation, we focused the DASH analysis first on the ring dihedrals Φ/Ψ 2 to 6 (T10). Each DASH state now represents the ensemble of similar ring-backbone conformations shown in Fig. 3 and Table 2. In order to distinguish between DASH overall states and DASH ring states, DASH overall states are denoted as T16 and DASH ring states as T10.

The initial 35 overall states are now reduced to 12 ring states. These ring states can be assigned clearly to the main time-windows of the trajectory between the transitions at 1.46, 5.90, 6.43, and 7.10 μs (Fig. 1a–c). Furthermore, analyzing the T10 and T16 DASH state trajectories (Fig. 4, Table S2), shows that each overall state can be assigned to a distinct ring state (see Table 2). In other words, each overall state can be considered as a main ring conformation combined with a distinct tail-conformation, as will be discussed in detail below.

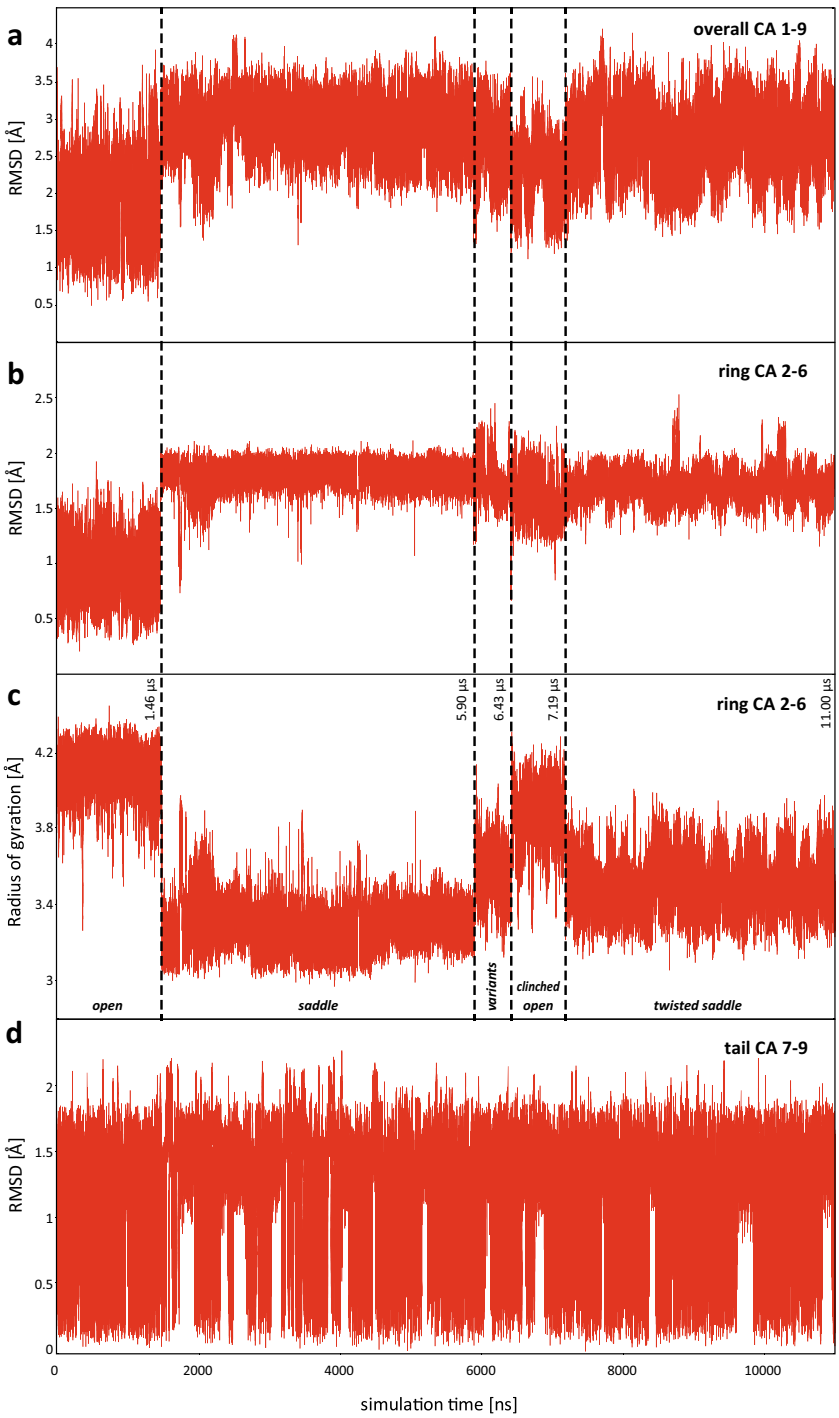

Fig. 1a–d Root mean square deviations (RMSD) and radius of gyration (RadGyr) of 8-Arg-vasopressin (AVP) during 11 μs molecluar dynamics (MD) simulation (reference: minimized initial MD structure, AVP_{1YF4}). **a** RMSD of Cα-backbone atoms 1–9 (*overall*). **b** RMSD of Cα-backbone atoms 2–6 (*ring*). **c** Radius of gyration of Cα-backbone atoms 2–6 (*ring*). **d** RMSD of Cα-backbone atoms 7–9 (*tail*). *Dotted lines* denote significant changes of the RMSD/RadGyr and mark time-windows of different ring conformations (denoted as *open*, *saddle*, *variants*, *clinched open* and *twisted saddle*)

Table 2 shows absolute and relative populations of overall and ring states and how they correspond. Absolute populations refer to the total simulation time of 11 μs and relative populations refer to the individual lengths of a conformational time-window. The main ring conformations and the corresponding main windows are denoted as (1) *open* (0 to 1.46 μs), (2) *saddle* (1.46 to 5.90 μs), (3) *clinched open* (6.43 – 7.19 μs) and (4) *twisted saddle* (7.19–11 μs) to reflect common structural characteristics. The fifth window identified on the RMSD plot between 5.90 and 6.43 μs contains variants of the main ring conformations and will not be discussed in detail here. This work is focused on the main conformational states of AVP, which correspond to the four main trajectory windows. Other, short-lived states are observed during the simulation, but do not play a significant role and will be defined only in the Supporting Information.

Table 1 Average root mean square deviations (avRMSD) and average radii of gyration (avRadGyr) for significant trajectory time-windows and backbone Cα alignments of 8-Arg-vasopressin (AVP). For abbreviations, see glossary

		trajectory time window [μs]				
	Alignment	0-1.46 *Open*	1.46-5.90 *Saddle*	5.90-6.43 *Variants*	6.43-7.19 *Clinched open*	7.1-11.00 *Twisted open*
avRMSD [Å]	*Overall*[a]	1.825	2.930	2.683	2.274	2.756
	Ring[b]	0.950	1.807	1.765	1.592	1.717
	Tail[c]	0.991	1.157	1.102	1.164	1.068
avRadGyr [Å]	*Ring*	4.077	3.278	3.569	3.870	3.500

[a] Cα 1–9 alignment

[b] Cα 1–6 alignment

[c] Cα 7–9 alignment

Populations of the conformations

The four main ring conformations (*open*, *saddle*, *clinched open* and *twisted saddle*) are present for more than 95 % of the simulation time. As a result of the DASH ring analysis, every conformational group is represented by two ring states (T10): a main state with a relative population of up to 94 % and a less populated state. Both major and minor states are present for 95 % to 100 % of the relevant time-window. Figure 3 shows the Cα 1–6 alignment of the ring states for each main ring conformation. Frequent interconversions between the representative states occur within each main conformational window. The DASH state mean angles (Table 3, Fig. 2) reveal that the major and minor ring-states of a distinct conformational group (*open* or *saddle*) differ significantly (more than 60°) for only one torsional angle. This is Φ6 for the *open* and *saddle* (differences of 72° and 66°, respectively; only 52° for *twisted saddle* and 35° for *clinched open*) states and Ψ5 (73°) for the *clinched open* states. The DASH state mean angles (Table 3, Figure S2) reveal that the major and

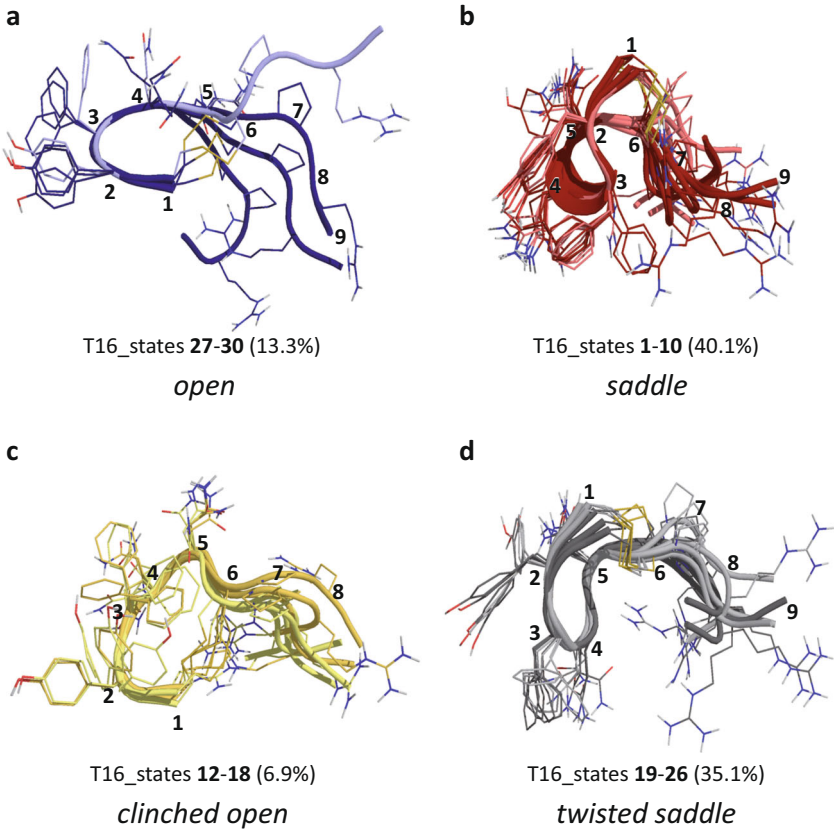

Fig. 2a–d Main overall conformations of AVP. **a**–**d** Representative states in water resulting from a DASH state analysis of backbone dihedrals Φ/Ψ 2–9. Absolute populations for every group of conformations are given in parenthesis and refer to 11 μs MD. Ring conformations: **a** *open*, **b** *saddle*, **c** *clinched open*, **d** *twisted saddle*. *Cartoon ribbon* backbone, *line notation* side chains; representatives are labeled only for the main populated state of each group. Residues are labeled only for each major populated state

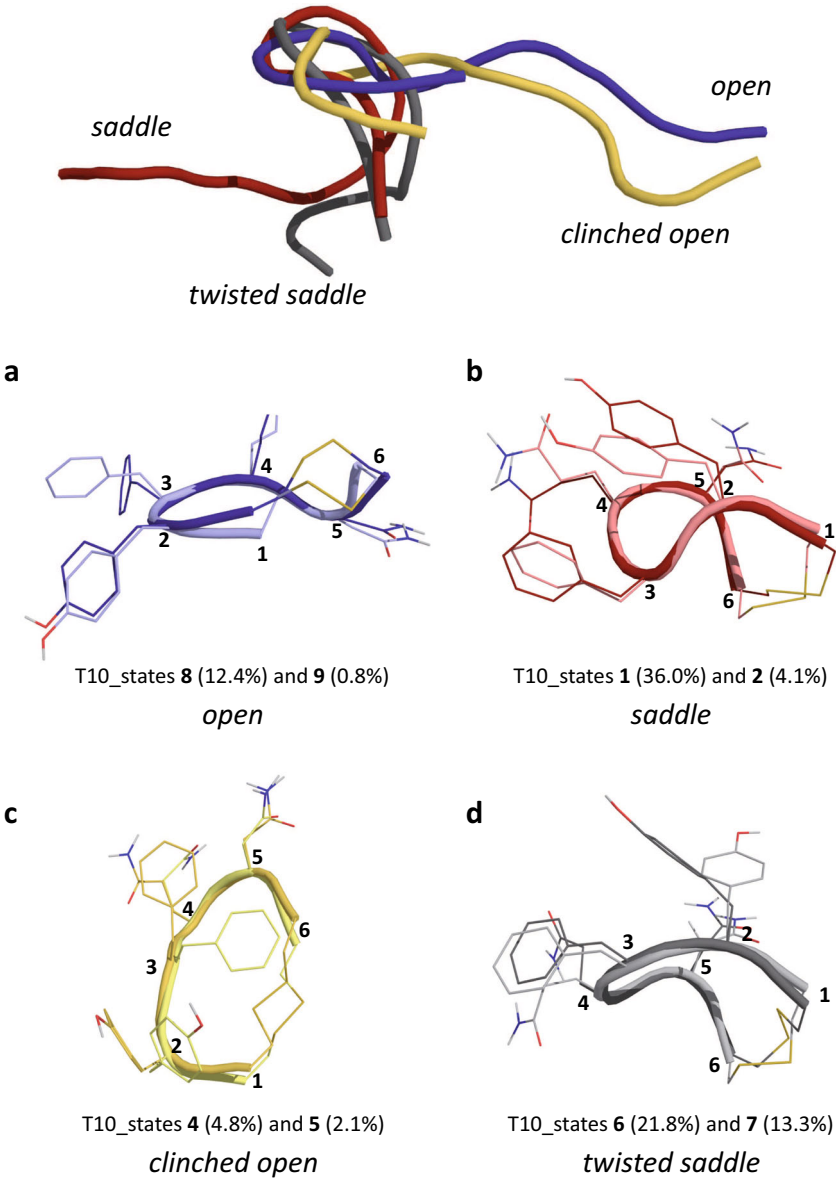

Fig. 3a–d Main ring conformations of AVP. Main representative ring states in water resulting from a DASH state analysis of backbone dihedrals Φ/Ψ 2–6. The absolute populations of each state during 11 μs MD are given in parenthesis. Ring states: **a** *open*, **b** *saddle*, **c** *clinched open*, **d** *twisted saddle*. *Cartoon ribbon* backbone, *line notation* side chains. Residues are labelled only for the major populated state each and the N-terminal tail is not shown in **a**–**d** for clarity. *Top panel* An illustration of the ring alignment of the backbone cartoons of the four main ring states (T10_8,1,4,6) including the tail

minor ring-states of a distinct conformational group (*open* or *saddle*) differ in only one torsion. This is Φ 6 for the *open*, *saddle* and *twisted saddle* states and Ψ 5 for the *clinched open* states. These result in different disulfide-bridge conformations for each state. Although the disulfide-bridge torsions were not included in the DASH ring-state analysis, their conformations are probably characteristic (see Fig. 3a–d, disulfide bridges are shown as lines). RMSD differences between states of the same ring conformation are small, ≤0.25 Å, in comparison to RMSD differences between states of different ring conformations, 0.9 to 2.2 Å (Table S3). The *saddle* and the *twisted saddle* ring conformations are the most populated structures, with absolute populations of 40 and 35 %, respectively. The open conformations, *open* and *clinched open*, occur only 13 % and 7 % of the time.

Secondary structure and hydrogen bonds

The secondary structure was determined by means of ring-internal turn propensities, turn types and hydrogen bonds. Turn propensities and hydrogen-bond occupancies were calculated using AMBER tools, and turn types were identified by comparing the DASH mean-angles with ideal β-turn type torsions. Turn propensities and hydrogen-bond populations are given in Tables 4 and 5 and the torsion-angle ensembles for every main DASH ring state in Table 3 and the results are illustrated in Scheme 1.

The *saddle* (Scheme 1b, Fig. 3b) and related *twisted saddle* (Scheme 1d, Fig. 3d) ring conformations are the most highly populated, occurring for 75 % of 11 μs (Table 2). Both feature a highly populated (more than 90 %) turn at residues Phe^3 and

Table 2 Representative states of the main overall and ring conformations of AVP. Listed are the population and conformational characteristics of the main overall states (T16) and ring states (T10) of AVP (minor and transient state variants: see Table S1). Absolute populations refer to 11 μs MD (100 %). Relative populations refer to the main time-windows of each conformational group (*open*, *saddle*, *clinched open* or *twisted saddle*). Characteristics of each ring conformation are given by β-turn types, turn centers, and transannular hydrogen bonds (Hbonds). T16= overall states defined by Φ/Ψ 2 to 9; T10=ring states defined by Φ/Ψ 2 to 6

	State population (T16)			State population (T10)		Conformational characteristics		
T16 state	Abs (%)	Rel (%)	T10 state	Abs (%)	Rel (%)	β-turn type[a]	Turn center	H bonds[b]
Open (0 to 1.455 μs = 1.455 μs)								
27	8.62	64.74	8	12.40	93.75			
28	3.25	24.60	8					
29	0.65	4.95	8					
30	0.75	5.70	9	0.83	6.25			
Total	13.28	100.00		13.23	100.00	no classical turns	2,3	(Tyr^2OGln^4NH)
Saddle (1.455 to 5.900 μs =4.445 μs)								
1	0.95	2.34	1	35.97	89.02			
2	0.74	1.82	1					
3	19.65	48.63	1					
4	7.88	19.51	1					
5	1.22	3.03	1					
6	5.60	13.87	1					
7	3.07	7.60	2	4.10	10.13			
8	0.35	0.87	2					
9	0.35	0.87	2					
10	0.25	0.62	2					
Total	40.06	99.15		40.07	99.16	I/(I)	3,4/4,5	Tyr^2OAsn^5NH, Tyr^2OCys^6NH
Clinched open (6.429 to 7.187 μs =0.758 μs)								
12	1.87	27.18	4	4.80	69.66	(VIII)		
13	1.41	20.45	4					
14	1.45	20.98	4					
15	0.23	3.30	5	2.09	30.34	I		
16	0.89	12.93	5					
17	0.62	8.97	5					
18	0.43	6.20	5					
Total	6.89	100.00		6.89	100.00	(VIII) /I	4,5	(Phe^3OCys^6NH)
Twisted saddle (7.187 to 11.000 μs =3.813 μs)								
19	14.04	36.32	6	21.8	57.62			
20	3.24	9.34	6					
21	0.85	2.44	6					
22	3.81	9.91	6					
23	0.26	0.76	7	13.33	37.11			
24	9.84	27.98	7					
25	2.07	5.01	7					
26	1	2.86	7					
total	35.10	94.62		35.13	94.73	II	3,4	Tyr^2OAsn^5NH
Σtotal	95.33			95.32				

[a] Parentheses indicate distorted versions of ideal β-turn types

[b] Hydrogen bonds in parenthesis are populated only 20-40 %

Gln^4. The *saddle* is characterized by a further turn centered at Asn^5 (89 %). This turn also occurs in the *twisted saddle* but is less highly populated (62 %). The DASH-state mean-angles (Table 3 and S4) reveal a β-turn type I centered at 3,4 for the

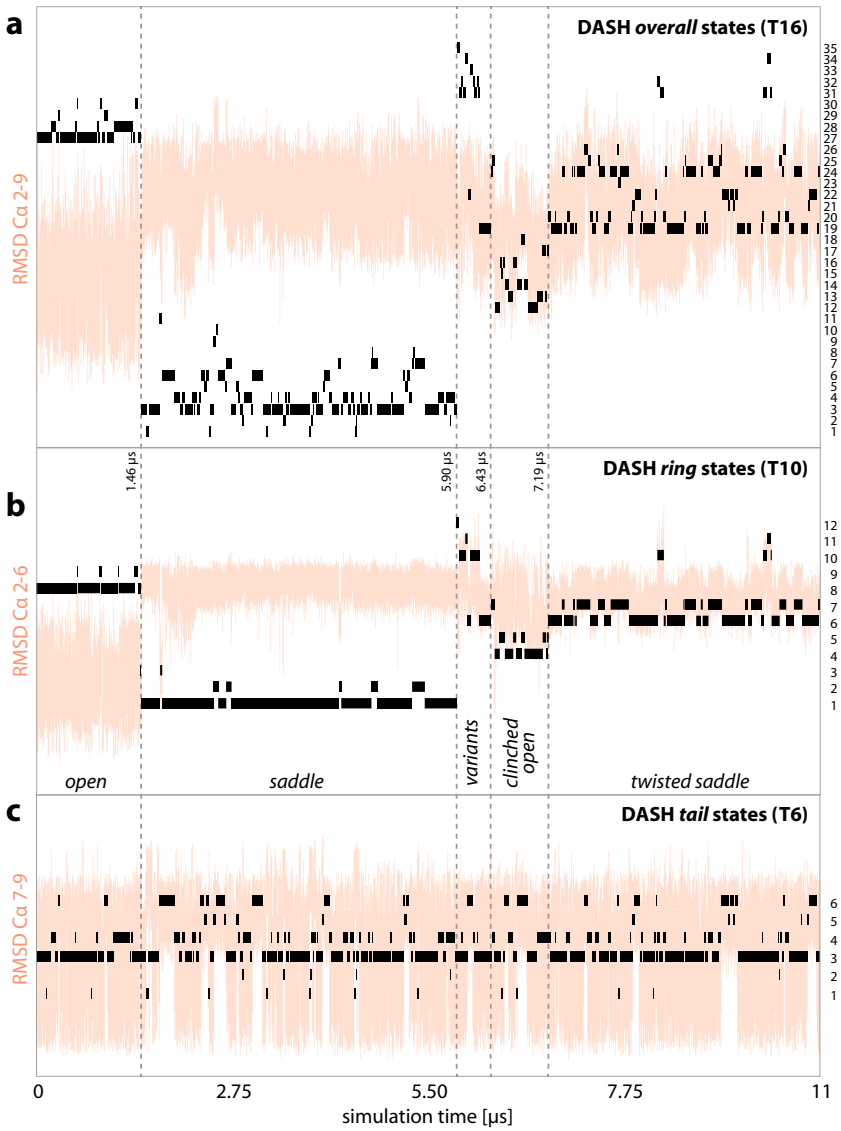

Fig. 4 DASH state trajectories for **a** *overall* (T16), **b** *ring* (T10), and **c** *tails* (T6) states. For a better understanding, the corresponding RMSD trajectories for *overall* (Cα 2–9), *ring* (Cα 2–6) and *tail* (Cα 7–9) alignments are shown in the background. States are numbered consecutively on the second *y*-axis, thus every horizontal line is the trajectory of a single DASH state and illustrates its individual distribution during the simulation. The transitions between time-windows of main ring conformations are marked with *vertical dashed lines*

saddle conformation in addition to a slightly distorted β-turn type I centered at 4,5. These β-turns are stabilized by highly populated (83–96 %) hydrogen bonds between the carbonyl-oxygen of Tyr^2 (Tyr^2O) and the amide-hydrogen of Asn^5 (Asn^5NH), and between Tyr^2O and Cys^6NH. In the *twisted saddle* ring-conformation, however, only the Tyr^2O-Asn^5NH hydrogen bond is highly populated (83 %) and the 3,4 centered turn is now a classical β-turn type II. The difference between a β-turn type I and type II is simply the orientation of the central peptide bond 3,4. The *twisted saddle* conformation shows a slight tendency to form a Tyr2NH-Asn5O hydrogen bond (7 % occupancy). A Tyr2NH-Asn5O hydrogen bond has also been suggested on the basis of NMR experiments [24]. A rearrangement from *saddle* to *twisted saddle* or changing the 3,4 β-turn from type I to type II twists the ring making it more open (cf. radius of gyration, Fig. 1c), whereas the main orientation of the side chains 2 to 4 remains unchanged. This may be necessary to facilitate AVP entry and/or fit into different GPCR pockets.

There is no direct transition between *saddle* and *twisted saddle* in the 11 µs MD, suggesting that interconversion of the two ring conformations may occur via one or more conformational intermediates, e.g., the *clinched open* conformation or the variants that are observed between 5.90 and 6.43 µs.

The relatively sparsely populated *clinched open* ring conformation (Scheme 1c, Fig. 3c) is significantly less folded than the two *saddle* conformations but more than the *open*. The most highly populated intramolecular hydrogen-bond is Phe^3O-Cys^6NH (28 %, Table 5) and turns centered at Gln^4 and Asn^5 occur about half of the time (46 %, Table 4). Loosely defined turns are thus more likely than ideal β-turns. The DASH ring-state mean-angles show a very high fluctuation of Ψ 5 (standard deviation=±61°, Table 3) so unambiguous turn-type assignment is not possible. The *clinched open* ring

Table 3 DASH state mean angles (Φ/Ψ) of the main ring states (T10) of AVP. Ideal Φ/Ψ (i+1, i+2): β-turn type I (−60°, −30°, −90°, 0°), type II (−60°, +120°, +80°, 0°), type VIII (-60°, -30°, -120°, 120°) [50, 51]. *SD* Standard deviation

T10 state	Tyr^2 Φ	Tyr^2 Ψ	Phe^3 Φ	Phe^3 Ψ	Gln^4 Φ	Gln^4 Ψ	Asn^5 Φ	Asn^5 Ψ	Cys^6 Φ	Cys^6 Ψ
Open										
8	−112.54	134.53	55.31	3.41	−135.33	152.15	−75.09	124.68	−127.16	148.39
SD	37.81	18.46	9.08	31.34	23.92	18.2	18.32	32.08	31.88	23.33
9	−98.98	129.37	56.09	0.76	−135.73	153.49	−66.41	113.78	−55.29	126.93
SD	54.64	26.48	9.27	31.72	23.88	23.1	31.29	80.23	61.52	40.84
Saddle										
1	−80.2	143.87	−62.88[a]	−21.36[a]	−86.73[a]	−7.38[a]	−113.37[a]	−27.13[a]	−126.42	133.12
SD	20.52	12.37	9.44	13.4	17.2	16.94	21.14	22.14	20.16	33.23
2	−84.29	147.09	−57.99[a]	−27.01[a]	−85.13[a]	−7.63[a]	−122.03[a]	−6.72[a]	−60.49	142.38
SD	23.05	13.93	10.95	15.59	17.53	16.62	20.55	41.47	32.18	24.51
Clinched open										
4	−95.37	−19	−101.27	156.57	−67.65	−19.06	−112.46	86.89	−117.42	145.84
SD	28.15	22.75	29.46	14.56	16.85	23.84	28.66	61.3	36.21	21.54
5	−90.52	−18.35	−116.2	151.18	−68.06	−20.5	−88.17	14.01	−82.72	144.88
SD	28.3	18.64	30.65	13.16	22.02	26.74	20.39	33.03	29.6	16.17
Twisted saddle										
6	−86.02	162.33	−52.48[a]	127.66[a]	55.04[a]	12.34[a]	−107.29	−7.44	−122.17	144.18
SD	29.44	13.88	16.16	14.69	9.01	21.14	29.86	48.29	28.23	23.53
7	−115.65	174.87	−52.78[a]	129.79[a]	57.39[a]	8.38[a]	−114.1	−16.45	−70.67	148.3
SD	24.26	19.63	19	13.91	8.24	20.56	25.07	29.84	19.33	13.72

[a] Torsions corresponding to β-turns (turn propensity >80 %, turn propensity 40–65 %)

structure can be classified as a flexible ring conformation with a tendency to form a β-turn type VIII or type I centered at 4,5.

Finally, the *open* ring conformation, the starting conformation for the simulation, shows none of the ideal turn structures (Scheme 1a, Fig. 3a). There is a slight tendency to center ring turns at residues Tyr^2 and Phe^3 (20 %, Table 5) accompanied by sparsely populated hydrogen bonding-interactions of Tyr^2O and Gln^4NH (39 %), and Cys^1O and Gln^4NH (12 %). Summarizing, this ring conformation can be readily classified as *open* as it has no significantly populated intramolecular hydrogen bonds and no defined β-turns.

Table 4 Turn propensities [%] for the main ring conformations of AVP

Turn center	Main ring conformation / trajectory time-window			
Residue	*Open*	*Saddle*	*Clinched open*	*Twisted saddle*
Cys^1	0.00	0.00	0.00	0.00
Tyr^2	20.20	0.00	0.00	0.18
Phe^3	20.20	94.10[a]	0.03	90.57[a]
Gln^4	0.08	93.93[a]	46.28	93.80[a]
Asn^5	0.07	89.33[a]	46.28	61.93[a]
Cys^6	0.00	2.53	0.00	0.01
Pro^7	3.80	18.57	20.99	10.82
Arg^8	3.80	17.32	20.99	10.82
Gly^9	0.00	0.00	0.00	0.00

[a] Torsions corresponding to β-turns

Transition key torsions

A torsion angle is defined as a key torsion if its value changes significantly (>90°) from one ring conformation to another. Figure 5 shows the differences of the mean torsions for the main ring conformations *open*, *saddle*, *clinched open* and *twisted saddle* represented by the main ring states (T10, Table 2). Only dihedrals Φ 2, Φ 5 and Φ/Ψ 6 do not show large differences, all other torsions can be qualified as key torsions for interconversions between the main ring conformations. A complete list of key torsion angle differences between main ring conformations is given in Table S5. Direct transitions only occurred between (1) *open* and *saddle* and (2) *clinched open* and *twisted saddle*. The key torsions for these transitions are (1) Φ 3, Ψ 4, Ψ 5 (Scheme 3a,b) and (2) Ψ 2, Φ 4, Ψ 5 (Scheme 3c, d). Changes of these torsions correlate with rotations of the corresponding peptide bonds and the relative orientation of carbonyl oxygens and amide hydrogens, and elucidate the mechanism of interconversions.

For example, to convert *open* to *saddle*, the Tyr^2 carbonyl-oxygen and the amide hydrogens of Asn^5 and Cys^6 should

Table 5 Occupancies of intramolecular hydrogen bonds (%) and corresponding turn centers for the main ring conformations of AVP

H-bond		Main ring conformation / Trajectory time-window				Turn center
O…	…HN	*open*	*saddle*	*cl.open*	*tw.saddle*	residues
Cys^1	Gln^4	12.03	0.00	0.00	2.24	2, 3
Tyr^2	Asn^5	0.00	95.70	0.00	82.60	3, 4
Tyr^2	Cys^6	0.00	83.19	0.00	37.28	3, 4, 5
Tyr^2	Gln^4	38.57	2.04	0.01	0.02	3
Phe^3	Cys^6	0.00	4.86	27.93	0.04	4, 5
Phe^3	Asn^5	0.13	2.41	10.21	23.83	4
Gln^4	Cys^6	8.78	0.06	18.67	1.60	5
Asn^5	Tyr^2	0.00	0.22	0.00	6.59	3, 4
Cys^6	Gly^9	2.20	10.82	12.11	5.67	7, 8

point into the ring. Torsions Φ 3, Ψ 4 and Ψ 5 are the key torsions responsible for turning these atoms into the ring and thus to enable the characteristic intramolecular hydrogen bond to be formed. To interconvert from *clinched open* to *twisted saddle*, the hydrogen bond Phe^3O–Cys^6NH must be replaced by one between Tyr^2O and Asn^5NH. This is accomplished by rotating Ψ 2 and Φ 4, which turns Tyr^2O into the ring displacing Phe^3O. A concomitant rotation of Ψ 5 causes Cys^6NH to turn thereby weakening the hydrogen bond between Phe^3O and Cys^6NH. These ring interconversions have so far proved too complex for their thermodynamics to be determined by simple umbrella sampling and are therefore now being investigated using dual-topology thermodynamic integration.

Disulfide bridge

One remaining important feature of the ring conformations is the chiral disulfide dihedral χ 3 (∠ Cys^2Cβ-Cys^2S-Cys^6S-Cys^6Cβ). Figure 6 shows the dynamics of this torsion. The disulfide bridge adopts two main conformations for χ 3 with average values of either +88.9° (g) or −86.6° (g′). Interconversions between these two states do not necessarily correspond to transitions between different time-windows of the ring conformations but are rather frequent independent occurrences. Each main ring conformation can exhibit conformations of the disulfide bridge conformations with negative and positive dihedrals. Transitions between these disulfide conformations occur independently of the main ring conformation. The positive torsion angle is favored by 78.2 to 21.8 % and is consistent with experimental evidence (see e.g., [49]). The simulation suggests that g/g′ transitions are more frequent for *open* ring conformations than for *saddle*.

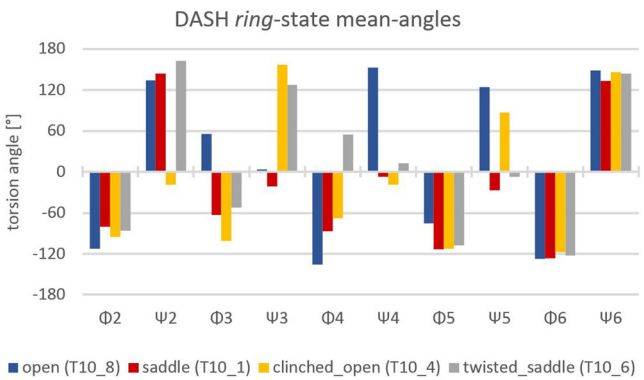

Fig. 5 DASH state mean angles (Φ/Ψ) of the main ring conformations of 8-Arg-vasopressin *open*, *saddle*, *clinched open*, and *twisted saddle* represented by the main ring states T10_8, 1, 4, and 6

Tail conformations

As described above, the RMSD trajectory of the Cα 7 to 9 segment (Fig. 1d) suggests two equally distributed main conformations for the tail, whereas the DASH analysis of the *tail* dihedrals Φ/Ψ 7 to 9 allows these dynamic conformations to be classified in detail. The results are given in Table 6, Scheme 2 and Fig. 7. There are six distinct tail states (T6) that reveal two major tail conformations, (1) an *extended* tail conformation with no significant turns, and (2) a tail conformation with a 7,8 β-turn type II, here denoted as *folded*. Each main conformation is represented by two DASH states, differing in torsions Φ/Ψ 9 (Fig. S3). These torsions are only responsible for the orientation of the C-terminal $CONH_2$-group and do not affect the *extended* or *folded* conformation.

AVP favors the *extended* conformation of the tail significantly with an absolute population of 81 % during the simulation versus 17 % for the *folded* 7,8 β-turn type II conformation. The preference for the *extended tail* conformation is due most likely to the bulky residue Arg^8, which causes steric clashes when the tail is *folded*.

Two further transient conformations can be identified: a hybrid tail conformation (absolute population 2.0 %), which is not completely extended but has no defined folding; and a 7,8 β-turn type I structure (absolute population 0.8 %).

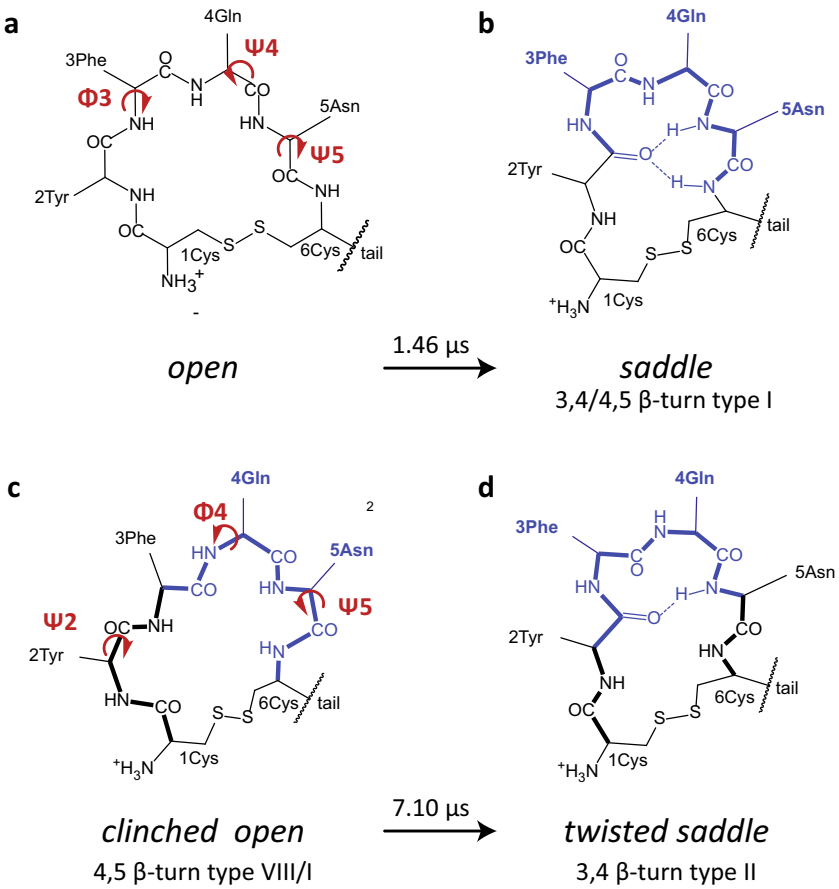

Scheme 3a–d Key torsions for the interconversion of the main ring conformations of AVP. **a**, **b** Interconversion *open* to *saddle* at 1.46 µs (11 µs MD). **c**,**d** Interconversion *clinched open* to *twisted saddle* at 7.10 µs (11 µs MD)

Figure 4 shows the DASH state trajectories for all *overall* states (T16), *ring* states (T10) and *tail* states (T6). There are 176 transitions between the 6 T6 *tail*-states but only 77 transitions between the 12 T10 *ring*-states, confirming that the tail is significantly more flexible than the ring. The most striking result, however, is that the *tail* states do not correlate directly with *ring* states in terms of transitions or formation of distinct conformational groups. In fact, like the two states of the disulfide bridge, all *tail* states are distributed evenly over the entire simulation independently of the ring conformation. This is shown convincingly by a PCA of the torsion angles throughout the simulation. As is shown in Fig. 8a, there are six significant PCs according to the eigenvalue-one test, of which PCs 5 and 6 have eigenvalues just barely larger than

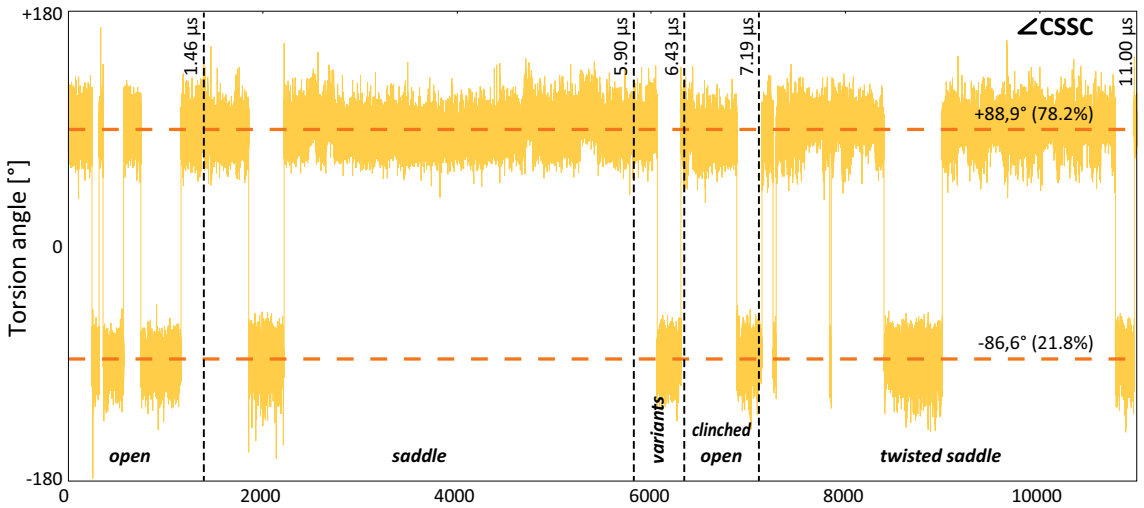

Fig. 6 Trajectory of the disulfide-bridge torsion Cys2χ3 (∠CSSC). *Horizontal dashed lines* average disulfide bridge torsions, *vertical dashed lines* transitions between time-windows of main ring conformations

Table 6 Population and distribution of tail conformations. The first column contains the DASH states (T6) that represent the tail conformations of AVP during 11 μs MD simulation. Absolute populations refer to the total simulation time of 11 μs. Relative populations refer to the time-windows of the main ring conformation (*open*, *saddle*, *clinched open*, and *twisted saddle*)

T6 state[a]	Tail state population (T6)				
	(0–11.0 μs) Abs (%)	*Open* (0–1.46 μs) Rel (%)	*Saddle* (1.46-5.90 μs) Rel (%)	*Clinched open* (6.43-7.19 μs) Rel (%)	*Twisted saddle* (7.19-11.00 μs) Rel (%)
Extended					
3	61.44	69.22	56.02	37.99	68.34
4	19.59	24.39	20.32	30.35	15.10
Total	81.03	93.61	76.34	68.34	83.44
7,8 β-turn type II					
5	2.52	0.00	3.87	0.00	2.75
6	13.61	4.91	15.31	26.12	12.51
Total	16.13	4.91	19.18	26.12	15.26
7,8 β-turn type I					
2	0.83	0.00	1.82	0.00	0.28
Distorted turn					
1	2.00	1.48	2.66	5.54	1.02
Σ Total	100.00	100.00	100.00	100.00	100.00

[a] Tail states defined by Φ/Ψ 7 to 9

unity and are therefore at best marginally non-trivial. Figure 8b shows the weights (squared coefficients) of the contributions of the individual torsions to PCs 1 and 2 and Fig. 8c those of PCs 3 and 4. The former are clearly localized on the ring and the latter on the tail. The contributions of ring torsions in PCs 3 and 4 and of tail fluctuations in 1 and 2 are very small. Interactive 3D-plots of the first four PCs are given as HTML-pages in the Supporting Material. Interestingly, these show that the two twisted saddle states, although very similar, are clearly separated in PC-space. This separation is due mostly to PC2.

Thus, every *overall* state can be described in a modular manner as a combination of a *ring* and a *tail* state. The matrix of all main-state combinations found in this simulation is given in Table 7. Although the conformational changes of the ring and tail are not correlated, the relative populations of *extended* and *folded* tail-states vary depending on the *ring* conformation (see Table 6). The highest preference for a *folded* tail is found for the *clinched open* ring (26 % relative population), the lowest (5 %) for an *open* ring conformation. The *saddle* and *twisted saddle ring* conformations are found together with a *folded* tail 20 % and 15 % of their occurrence, respectively. Again, the sterically demanding Arg[8] residue is most likely responsible for these preferences; the propensity to form a folded tail depends on the available space.

Conclusions

A single long (11 μs) simulation of AVP in water has revealed details of its conformational behavior and possible biologically

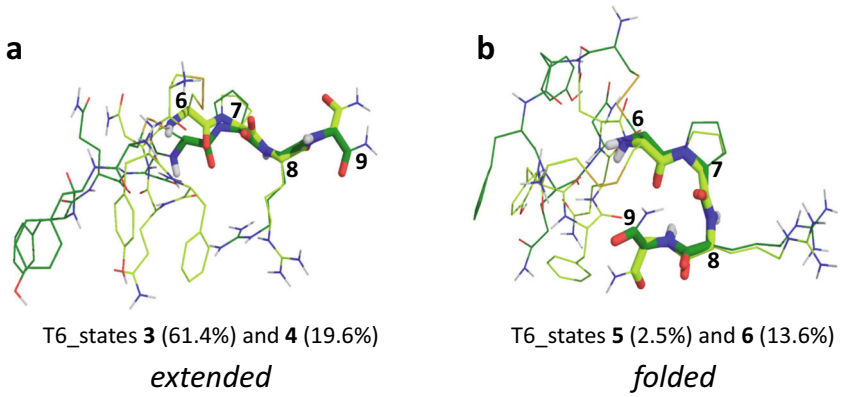

Fig. 7a,b Tail conformations of AVP. Main representative tail states resulting from a DASH state analysis of backbone dihedrals Φ/Ψ 7 to 9. Absolute population are given in parenthesis. **a** *Extended* tail conformations. **b** *Folded* tail conformations with β-turn centered at residues 7 and 8. *Stick representation* tail, *line representation* ring and side chains. Residues are labeled only for each major populated state

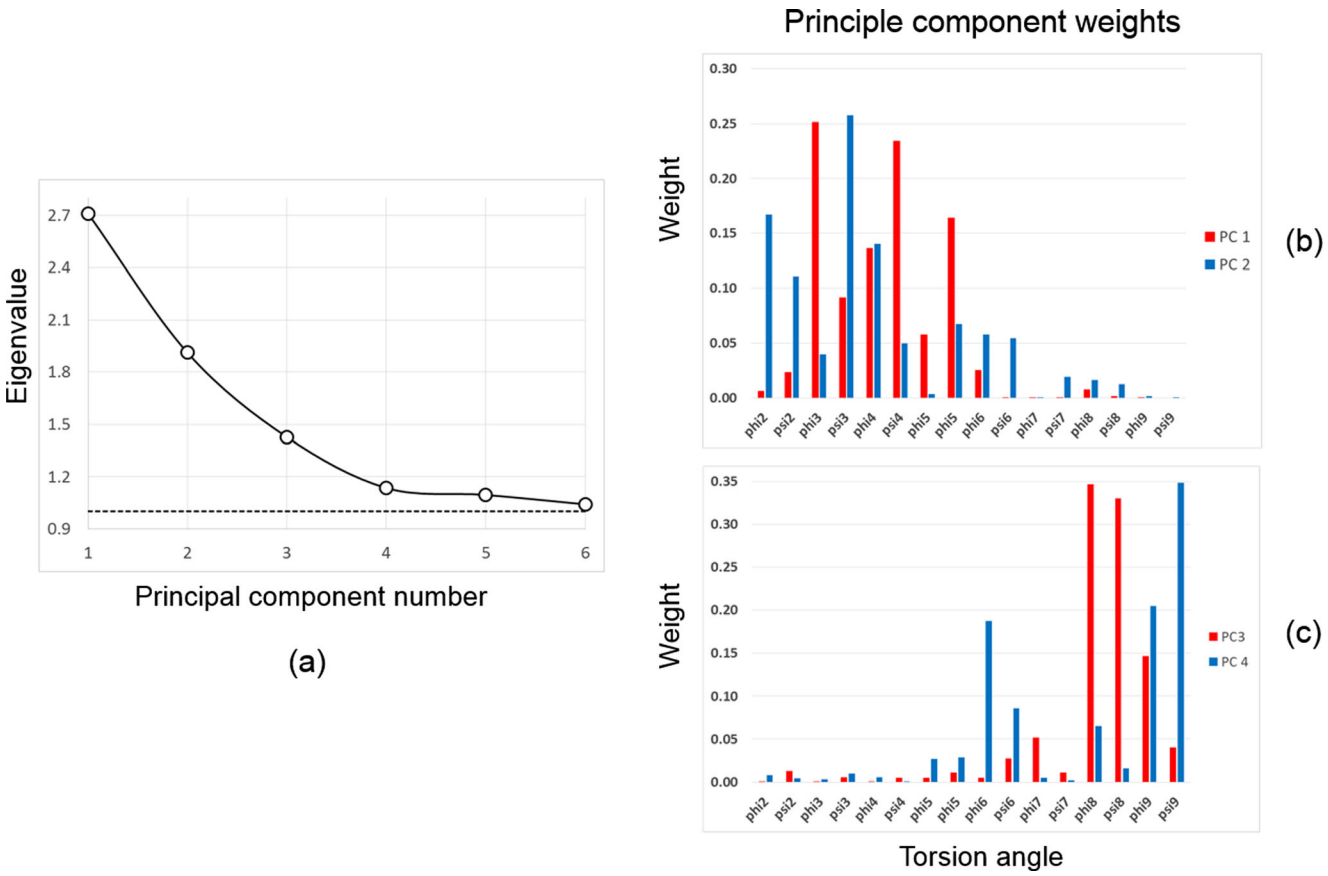

Fig. 8a–c Summaries of the principal component analysis (PCA) of the torsion angles during the simulation. **a** Eigenvalue plot. **b** Weights of the torsion angles for principal components (PCs) 1 and 2. **c** Weights of the torsion angles for PCs 3 and 4

active conformations. Conformational changes on the MD time scale are frustratingly slow, so that, even from the long simulation, we cannot estimate the free-energy difference between the ring conformations from their concentrations. However, the conformational rearrangements are clearly fast on the NMR time scale, in agreement with the experimental results.

The simulation reveals four distinct ring conformations that are essentially independent of the faster tail motions. The

Table 7 *Overall* State=*Ring* State+*Tail* State. A matrix of *overall* states (T16) as combination of the *ring* and *tail* states (T10 and T6) that represent the main ring and tail conformations (*open, saddle, clinched open, twisted saddle, extended,* and *folded*). The states result from DASH analyses of torsions Φ/Ψ 2 to 9 (T16, overall states), 2 to 6 (T10, ring states) and 7 to 9 (T6, tail states). The assignment is based on the corresponding DASH state trajectories. PDBs of all states are provided in the Supplementary Material

Overall states (T16) (T6 X T10)				Tail states (T6)			
				Extended		*7,8 β-turn II*	
				61.4 % 3	19.6 % 4	13.6 % 6	2.5 % 5
Ring states (T10)	*Open*	12.4 %	8	27	28	29	
		0.8 %	9	30	28		
	Saddle	36.0 %	1	3	4	6	5
		4.1 %	2	7	8	10	9
	Clinched open	4.8 %	4	12	13	14	
		2.1 %	5	16	17	18	
	Twisted saddle	21.8 %	6	19	20	22	21
		13.3 %	7	24	25	26	

saddle and *twisted saddle* ring conformations exhibit β-turns centered at residues 3,4/4,5 as expected from experiments and are fixed by transannular hydrogen bonds. The alternative *open* and *clinched open* conformation do not feature transannular H-bridges. The *saddle* structure identified in the simulation corresponds closely to that found in crystal structure 1JK4.

The simulation is quite consistent with Sikorska and Rodziewicz-Motowidlo's NMR results [25]. They suggest two main conformations, both with 3,4 β II-turns. One is proposed to exhibit a 4,5 β III′-turn and the other a type I′-turn at this position. Our simulations also reveal turns at 3,4 and 4,5 to be dominant in aqueous solution. The 3,4 β-turn type II is found in our *twisted saddle* conformation, but only with a sparsely populated 4,5 turn; a significantly high turn propensity at residues 4 and 5 is found in our *saddle* conformation but here in combination with a β-turn type I at residues 3 and 4. The two studies agree well about the tail conformation, which we found to be approximately 80 % *extended*.

The *open* structure featured in the simulation corresponds closely to the AVP conformation found in the crystal structure of the trypsin complex (PDB ID: 1YF4) and features neither a well characterized β-turn nor conserved transannular hydrogen bonds. The *clinched open* conformation identified in the simulation is apparently new and probably represents an intermediate minority conformation involved in inter-*saddle* rearrangements.

In general, the simulation is compatible with the known experimental data, which allows us to be confident about its accuracy, even though it is limited to 11 μs and exhibits only a few transitions between major rings states. Above all, the main conformations found can all be considered as candidates for biologically active conformations in their cognate receptors as they are clearly easily accessible thermodynamically. We are now carrying out extensive thermodynamic integration studies to define the thermodynamics of the major conformations in solution.

Technically, DASH has proven to be an extremely useful and effective analysis tool for such simulations. In particular its beneficial scaling helps to analyze such long simulations. The finding that the movements of the ring and the tail are largely independent facilitates the analysis considerably.

The conformational distribution demonstrated in this work can now serve as a basis for comparison with those simulated for AVP docked into receptor pockets and for extended simulations of NMR and circular dichroism spectra. Above all, however, MD simulations have proven once more to be useful, and perhaps the most powerful, tools for analyzing the conformational behavior of peptide hormones of comparable size to AVP.

Acknowledgments This work was supported by the European project "Peptide Research Network of Excellence" PeReNE as part of the Interreg IVA France (Channel)—England 2007–2014 program (Interreg EU). We thank Jonathan Essex (University of Southampton, UK) and Ronan Bureau (University of Caen, France) for helpful discussions and Harald Lanig (University of Erlangen, Germany) for support with the simulations. Work in Erlangen was supported by the Deutsche Forschungsgemeinschaft as part of Graduiertenkolleg 1910 "*Medicinal Chemistry of Selective GPCR Ligands*".

Glossary

Abs	Absolute
AMBER	Assisted Model Building with Energy Refinement
av	Average
AVP	8-Arginine-Vasopressin
cl.open	Clinched Open
DASH	Dynamics Analysis by Salt and Hudson
DMS	Dimethyl Sulfate
ff99sb	Force Field 1999 Stony Brooks
g/g′	gauche/gauche′
GPCR	G-Protein Coupled Receptor
Hbond	Hydrogen Bond
MD	Molecular Dynamics
NH	Amide Hydrogen
NP	Neurophysin
O	Carbonyl Oxygen
OT	Oxytocin
PC	Principle Component
PCA	Principle Component Analysis
PDB	Protein Data Bank
RadGyr	Radius of Gyration
Rel	Relative
RMSD	Root Mean Square Deviation
SDS	Sodium Dodecyl Sulfate
StdDev	Standard Deviation
T10	DASH analysis of torsions Φ/Ψ 2 to 6 (10 torsions)
T16	DASH analysis of torsions Φ/Ψ 2 to 9 (16 torsions)
TIP4P-Ew	Transferable Intermolecular Potential 4 Point - Ewald
TM	Trans Membrane
tw.saddle	Twisted Saddle
V2R	Vasopressin-2 receptor

References

1. du Vigneaud V, Gish DT, Katsoyannis PG (1954) A Synthetic Preparation Possessing Biological Properties Associated with Arginine Vasopressin. J Am Chem Soc 76:4751–4752

2. Laycock JF (2010) Perspectives on vasopressin. Imperial College Press, London
3. Gimpl G, Fahrenholz F (2001) The oxytocin receptor system: structure, function, and regulation. Physiol Rev 81:629–683
4. Strand FL (1999) Neuropeptides: regulators of physiological processes. MIT Press, Cambridge, pp 229–265
5. Barberis C, Morin D, Durroux T, Mouillac B, Guillon G, Seyer R, Hibert M, Tribollet E, Manning M (1999) Molecular pharmacology of AVP and OT receptors and therapeutic potential. Drug News Perspect 12:279–292
6. Wu CK, Hu B, Rose JP, Liu ZJ, Nguyen TL, Zheng C, Breslow E, Wang BC (2001) Structures of an unliganded neurophysin and its vasopressin complex: implications for binding and allosteric mechanisms. Protein Sci: Publ Protein Soc 10:1869–1880
7. Fujiwara Y, Tanoue A, Tsujimoto G, Koshimizu TA (2012) The roles of V1a vasopressin receptors in blood pressure homeostasis: a review of studies on V1a receptor knockout mice. Clin Exp Nephrol 16:30–34
8. Pittman QJ, Bagdan B (1992) Vasopressin involvement in central control of blood pressure. Prog Brain Res 91:69–74
9. Pittman QJ, Wilkinson MF (1992) Central arginine vasopressin and endogenous antipyresis. Can J Physiol Pharmacol 70:786–790
10. Mogil JS, Sorge RE, LaCroix-Fralish ML et al (2011) Pain sensitivity and vasopressin analgesia are mediated by a gene-sex-environment interaction. Nat Neurosci 14:1569–1573
11. Manning M, Misicka A, Olma A et al (2012) Oxytocin and vasopressin agonists and antagonists as research tools and potential therapeutics. J Neuroendocrinol 24:609–628
12. Jard S (1998) Vasopressin receptors. A historical survey. Adv Exp Med Biol 449:1–13
13. Dunning BE, Moltz JH, Fawcett CP (1984) Modulation of insulin and glucagon secretion from the perfused rat pancreas by the neurohypophysial hormones and by desamino-D-arginine vasopressin (DDAVP). Peptides 5:871–875
14. Young LJ, Flanagan-Cato LM (2012) Editorial comment: oxytocin, vasopressin and social behavior. Horm Behav 61:227–229
15. Insel TR, O'Brien DJ, Leckman JF (1999) Oxytocin, vasopressin, and autism: is there a connection? Biol Psychiatry 45:145–157
16. Yamaguchi Y, Suzuki T, Mizoro Y, Kori H, Okada K et al (2013) Mice genetically deficient in vasopressin V1a and V1b receptors are resistant to jet lag. Science 342:85–90
17. Manning M, Chan WY, Sawyer WH (1993) Design of cyclic and linear peptide antagonists of vasopressin and oxytocin: current status and future directions. Regul Pept 45:279–283
18. Verbalis JG (2003) Disorders of body water homeostasis. Best Practice Res Clin Endocrinol Metab 17:471–503
19. Lehrich RW, Greenberg A (2012) Hyponatremia and the use of vasopressin receptor antagonists in critically ill patients. J Intensive Care Med 27:207–218
20. Verbalis JG (2006) AVP receptor antagonists as aquaretics: review and assessment of clinical data. Cleve Clin J Med 73(Suppl 3):S24–S33
21. Barlow M (2002) Vasopressin. Emerg Med (Freemantle) 14:304–314
22. Syed Ibrahim B, Pattabhi V (2005) Trypsin inhibition by a peptide hormone: crystal structure of trypsin-vasopressin complex. J Mol Biol 348:1191–1198
23. Rose JP, Wu CK, Hsiao CD, Breslow E, Wang BC (1996) Crystal structure of the neurophysin-oxytocin complex. Nat Struct Biol 3:163–169
24. Schmidt JM, Ohlenschlager O, Ruterjans H et al (1991) Conformation of [8-arginine]vasopressin and V1 antagonists in dimethyl sulfoxide solution derived from two-dimensional NMR spectroscopy and molecular dynamics simulation. Eur J Biochem 201:355–371
25. Sikorska E, Rodziewicz-Motowidlo S (2008) Conformational studies of vasopressin and mesotocin using NMR spectroscopy and molecular modelling methods. Part I: Studies in water. J Pept Sci 14:76–84
26. Rodziewicz-Motowidlo S, Sikorska E, Oleszczuk M, Czaplewski C (2008) Conformational studies of vasopressin and mesotocin using NMR spectroscopy and molecular modelling methods. Part II: Studies in the SDS micelle. J Pept Sci 14:85–96
27. Liwo A, Tempczyk A, Oldziej S et al (1996) Exploration of the conformational space of oxytocin and arginine-vasopressin using the electrostatically driven Monte Carlo and molecular dynamics methods. Biopolymers 38:157–175
28. Czaplewski C, Kazmierkiewicz R, Ciarkowski J (1998) Molecular modeling of the human vasopressin V2 receptor/agonist complex. J Comput Aided Mol Des 12:275–287
29. Mouillac B, Chini B, Balestre MN et al (1995) The binding site of neuropeptide vasopressin V1a receptor. Evidence for a major localization within transmembrane regions. J Biol Chem 270:25771–25777
30. Barberis C, Mouillac B, Durroux T (1998) Structural bases of vasopressin/oxytocin receptor function. J Endocrinol 156(2):223–229
31. Schwyzer R (1995) In search of the 'bio-active conformation'—is it induced by the target cell membrane? J Mol Recognit 8:3–8
32. Mierke DF, Giragossian C (2001) Peptide hormone binding to G-protein-coupled receptors: structural characterization via NMR techniques. Med Res Rev 21:450–471
33. Changeux JP, Edelstein SJ (2005) Allosteric mechanisms of signal transduction. Science 308:1424–1428
34. Cui Q, Karplus M (2008) Allostery and cooperativity revisited. Protein Sci: Publ Protein Soc 17:1295–1307
35. Gunasekaran K, Ma B, Nussinov R (2004) Is allostery an intrinsic property of all dynamic proteins? Proteins 57:433–443
36. Shao J, Tanner SW, Thompson N, Cheatham TE (2007) Clustering Molecular Dynamics Trajectories: 1. Characterizing the Performance of Different Clustering Algorithms. J Chem Theory Comput 3:2312–2334
37. Case DA, Darden TA, Cheatham II TE, et al (2008) AMBER 10. University of California, San Francisco
38. Case DA, Darden TA, Cheatham II TE, et al (2008) AmberTools 1.0. University of California, San Francisco
39. Salt DW, Hudson BD, Banting L et al (2005) DASH: a novel analysis method for molecular dynamics simulation data. Analysis of ligands of PPAR-gamma. J Med Chem 48:3214–3220
40. Jorgensen WL, Chandrasekhar J, Madura JD et al (1983) Comparison of Simple Potential Functions for Simulating Liquid Water. J Chem Phys 79:926–935
41. Horn HW, Swope WC, Pitera JW et al (2004) Development of an improved four-site water model for biomolecular simulations: TIP4P-Ew. J Chem Phys 120:9665–9678
42. Hornak V, Abel R, Okur A et al (2006) Comparison of multiple amber force fields and development of improved protein backbone parameters. Proteins Struct Funct Bioinforma 65:712–725
43. Berendsen HJC, Postma JPM, van Gunsteren WF et al (1984) Comparison of multiple amber force fields and development of improved protein backbone parameters. J Chem Phys 81:3684–3690
44. Ryckaert JP, Ciccotti G, Berendsen HJC (1977) Numerical-Integration of Cartesian Equations of Motion of a System with Constraints - Molecular-Dynamics of N-Alkanes. J Comput Phys 23:327–341

45. Darden T, York D, Pedersen L (1993) Particle mesh Ewald—an N.Log(N) method for Ewald sums in large systems. J Chem Phys 98:10089–10092
46. DASH 1.0 (2008) Available from: http://www.port.ac.uk/research/cmd/software
47. SAR-Caddle (2013) Cepos InSilico, Kempston, UK; Available from: http://www.ceposinsilico.de/products/sar-caddle.htm
48. Kaiser HF (1960) The application of electronic computers to factor analysis. Educ Psychol Meas 20:141–151
49. Pazderková M, Bednárová L, Dlouhá H et al (2012) Electronic and vibrational optical activity of several peptides related to neurohypophyseal hormones: disulfide group conformation. Biopolymers 97:923–932
50. Venkatachalam CM (1968) Stereochemical criteria for polypeptides and proteins. V. Conformation of a system of three linked peptide units. Biopolymers 6:1425–1436
51. Richardson JS (1981) The anatomy and taxonomy of protein structure. Adv Protein Chem 34:167–339